Search for Majorana Neutrinos Near the Inverted Mass Hierarchy Region with KamLAND-Zen

A. Gando,[1] Y. Gando,[1] T. Hachiya,[1] A. Hayashi,[1] S. Hayashida,[1] H. Ikeda,[1] K. Inoue,[1,2] K. Ishidoshiro,[1] Y. Karino,[1] M. Koga,[1,2] S. Matsuda,[1] T. Mitsui,[1] K. Nakamura,[1,2] S. Obara,[1] T. Oura,[1] H. Ozaki,[1] I. Shimizu,[1] Y. Shirahata,[1] J. Shirai,[1] A. Suzuki,[1] T. Takai,[1] K. Tamae,[1] Y. Teraoka,[1] K. Ueshima,[1] H. Watanabe,[1] A. Kozlov,[2] Y. Takemoto,[2] S. Yoshida,[3] K. Fushimi,[4] T. I. Banks,[5] B. E. Berger,[2,5] B. K. Fujikawa,[2,5] T. O'Donnell,[5] L. A. Winslow,[6] Y. Efremenko,[2,7] H. J. Karwowski,[8] D. M. Markoff,[8] W. Tornow,[2,8] J. A. Detwiler,[2,9] S. Enomoto,[2,9] and M. P. Decowski[2,10]

(KamLAND-Zen Collaboration)

[1]*Research Center for Neutrino Science, Tohoku University, Sendai 980-8578, Japan*
[2]*Kavli Institute for the Physics and Mathematics of the Universe (WPI), The University of Tokyo Institutes for Advanced Study, The University of Tokyo, Kashiwa, Chiba 277-8583, Japan*
[3]*Graduate School of Science, Osaka University, Toyonaka, Osaka 560-0043, Japan*
[4]*Faculty of Integrated Arts and Science, University of Tokushima, Tokushima 770-8502, Japan*
[5]*Physics Department, University of California, Berkeley, and Lawrence Berkeley National Laboratory, Berkeley, California 94720, USA*
[6]*Massachusetts Institute of Technology, Cambridge, Massachusetts 02139, USA*
[7]*Department of Physics and Astronomy, University of Tennessee, Knoxville, Tennessee 37996, USA*
[8]*Triangle Universities Nuclear Laboratory, Durham, North Carolina 27708, USA; Physics Departments at Duke University, Durham, North Carolina 27705, USA; and North Carolina Central University, Durham, North Carolina 27701, USA*
[9]*Center for Experimental Nuclear Physics and Astrophysics, University of Washington, Seattle, Washington 98195, USA*
[10]*Nikhef and the University of Amsterdam, Science Park, Amsterdam 1098XG, The Netherlands*

(Received 10 May 2016; revised manuscript received 21 June 2016; published 16 August 2016)

We present an improved search for neutrinoless double-beta ($0\nu\beta\beta$) decay of ^{136}Xe in the KamLAND-Zen experiment. Owing to purification of the xenon-loaded liquid scintillator, we achieved a significant reduction of the ^{110m}Ag contaminant identified in previous searches. Combining the results from the first and second phase, we obtain a lower limit for the $0\nu\beta\beta$ decay half-life of $T^{0\nu}_{1/2} > 1.07 \times 10^{26}$ yr at 90% C.L., an almost sixfold improvement over previous limits. Using commonly adopted nuclear matrix element calculations, the corresponding upper limits on the effective Majorana neutrino mass are in the range 61–165 meV. For the most optimistic nuclear matrix elements, this limit reaches the bottom of the quasidegenerate neutrino mass region.

DOI: 10.1103/PhysRevLett.117.082503

Neutrinoless double-beta ($0\nu\beta\beta$) decay is an exotic nuclear process predicted by extensions of the Standard Model of particle physics. Observation of this decay demonstrates the nonconservation of lepton number, and proves that neutrinos have a Majorana mass component. In the framework of light Majorana neutrino exchange, its decay rate is proportional to the square of the effective Majorana neutrino mass $\langle m_{\beta\beta}\rangle \equiv |\sum_i U_{ei}^2 m_{\nu_i}|$. Recent $0\nu\beta\beta$ searches [1] involving ^{76}Ge (GERDA [2]) and ^{136}Xe (KamLAND-Zen [3] and EXO-200 [4]) provide upper limits on $\langle m_{\beta\beta}\rangle$ of ~0.2–0.4 eV using available nuclear matrix element (NME) values from the literature. The sensitivities of these searches correspond to mass scales in the so-called quasidegenerate mass region.

KamLAND-Zen is a double-beta decay experiment that exploits the existing detection infrastructure and radiopurity of KamLAND [5,6]. The KamLAND-Zen detector consists of 13 tons of Xe-loaded liquid scintillator (Xe-LS) contained in a 3.08-m-diameter spherical inner balloon (IB) located at the center of the KamLAND detector. The IB is constructed from 25-μm-thick transparent nylon film and is surrounded by 1 kton of liquid scintillator (LS) contained in a 13-m-diameter spherical outer balloon. The outer LS acts as an active shield. The scintillation photons are viewed by 1879 photomultiplier tubes (PMTs) mounted on the inner surface of the containment vessel. The Xe-LS consists of 80.7% decane and 19.3% pseudocumene (1,2,4-trimethylbenzene) by volume, 2.29 g/liter of the fluor PPO (2,5-diphenyloxazole), and (2.91 ± 0.04)% by weight of isotopically enriched xenon gas. The isotopic abundances in the enriched xenon were measured by a residual gas analyzer to be (90.77 ± 0.08)% ^{136}Xe, (8.96 ± 0.02)% ^{134}Xe. Other xenon isotopes have negligible presence. The two electrons emitted from ^{136}Xe $\beta\beta$ decay

produce scintillation light and their summed energy is observed. Hypothetical $0\nu\beta\beta$ decays would produce a peak at the Q value of the decay, distinguishable from $2\nu\beta\beta$ decays that have a continuous spectrum.

In the first phase of KamLAND-Zen (phase I) [3], we obtained a lower limit of $T^{0\nu}_{1/2} > 1.9 \times 10^{25}$ yr (90% C.L.) on the ^{136}Xe $0\nu\beta\beta$ decay half-life. The sensitivity of the phase-I search was limited by the presence of an unexpected background peak, consistent with ^{110m}Ag β^- decay ($\tau = 360$ day, $Q = 3.01$ MeV), just above the 2.458 MeV Q value of ^{136}Xe $\beta\beta$ decay. After completing phase I, we embarked on a Xe-LS purification campaign that continued for 18 months. First, we extracted the Xe-LS in small batches from the IB through a teflon tube whose intake was near the bottom of the IB volume. We then isolated and stored the Xe before placing the Xe-depleted LS back in the top of the IB where it was later replaced by a new LS. This new LS was initially purified by water extraction followed by vacuum distillation. The replacement of the Xe-depleted LS was performed in three cycles equivalent to one IB volume exchange for each cycle. The LS was purified by vacuum distillation during each cycle. We also purified a mix of recovered and new Xe through distillation and refining with a heated zirconium getter. Finally, the Xe was dissolved into the purified LS. In December of 2013, we started the second science run (phase II), and found a reduction of ^{110m}Ag by more than a factor of 10. We report on the analysis of the complete phase-II data set, collected between December 11, 2013 and October 27, 2015. The total live time is 534.5 days after muon spallation cuts, discussed later. This corresponds to an exposure of 504 kg yr of ^{136}Xe with the whole Xe-LS volume.

Following the end of phase II, we performed a detector calibration campaign using radioactive sources deployed at various positions along the central axis of the IB. The event position reconstruction—determined from the scintillation photon arrival times—reproduces the known source positions to within 2.0 cm; the reconstruction performance is better than 1.0 cm for events occurring within 1 m of the IB center. The energy scale was studied using γ rays from ^{60}Co, ^{68}Ge, and ^{137}Cs radioactive sources, γ rays from the capture of spallation neutrons on protons and ^{12}C, and $\beta + \gamma$-ray emissions from ^{214}Bi, a daughter of ^{222}Rn ($\tau = 5.5$ day) that was introduced during the Xe-LS purification. The calibration data indicate that the reconstructed energy varies by less than 1.0% throughout the Xe-LS volume, and the time variation of the energy scale is less than 1.0%. Uncertainties from the nonlinear energy response due to scintillator quenching and Cherenkov light production are constrained by the calibrations. The light yield of the Xe-LS is 7% lower than that of the outer LS, which is corrected in the detector simulation, while the nonlinearities for both the LS regions are consistent. The observed energy resolution is $\sigma \sim 7.3\%/\sqrt{E(\mathrm{MeV})}$, slightly worse relative to phase I due to an increased number of dead PMTs.

We apply the following series of cuts to select $\beta\beta$ decay events. (i) The reconstructed vertex must be within 2.0 m of the detector center. (ii) Muons and events within 2 ms after muons are rejected. (iii) ^{214}Bi-^{214}Po ($\tau = 237$ μs) decays are eliminated by a delayed coincidence tag, requiring the time and distance between the prompt ^{214}Bi and delayed ^{214}Po decay events to be less than 1.9 ms and 1.7 m, respectively. The cut removes $(99.95 \pm 0.01)\%$ of ^{214}Bi-^{214}Po decays, where the inefficiency is dominated by the timing cut, and the uncertainty is estimated from analysis of periods with high Rn levels. The same cut is not effective for ^{212}Bi-^{212}Po ($\tau = 0.4$ μs) decays that occur within a single ~200-ns-long data acquisition event window. Therefore, the cut is augmented with a double-pulse identification in the photon arrival time distribution after subtracting the time of flight from the vertex to each PMT. The ^{212}Bi-^{212}Po rejection efficiency is $(95 \pm 3)\%$, confirmed with high-Rn data. (iv) Reactor $\bar{\nu}_e$'s identified by a delayed coincidence of positrons and neutron-capture γ's [6] are discarded. (v) Poorly reconstructed events are rejected. These events are tagged using a vertex-time-charge discriminator that measures how well the observed PMT time-charge distributions agree with those expected based on the reconstructed vertex [7]. The total cut inefficiency for $\beta\beta$ events is less than 0.1%.

Background sources external to the Xe-LS are dominated by radioactive impurities on the IB film. Based on a spectral fit to events reconstructed around the IB, we find that the dominant background sources are ^{134}Cs ($\beta + \gamma$, $\tau = 2.97$ yr) in the energy region $1.2 < E < 2.0$ MeV ($2\nu\beta\beta$ window), and ^{214}Bi in the region $2.3 < E < 2.7$ MeV ($0\nu\beta\beta$ window). The observed activity ratio of ^{134}Cs to ^{137}Cs (0.662 MeV γ, $\tau = 43.4$ yr) indicates that the IB film was contaminated by fallout from the Fukushima-I reactor accident in 2011 [8]. ^{214}Bi is a daughter of ^{238}U, a naturally occurring contaminant. The observed rate of ^{214}Bi decays indicates that the ^{238}U concentration in the nylon film is 0.16 ppb assuming secular equilibrium, while the *ex situ* measurement by ICP-MS yielded 2 ppt. The nonuniform ^{214}Bi event distribution observed on the IB indicates that this discrepancy is caused by dust contamination rather than decay chain nonequilibrium. Figure 1(a) shows the vertex distribution of candidate events, and the predicted ^{214}Bi background events from a Monte Carlo (MC) simulation in the $0\nu\beta\beta$ window. The z distribution of ^{214}Bi decays on the IB is evaluated from the data, and used for the radioactive decay model in the MC simulation. For the ^{214}Bi background, the vertex dispersion model was constructed from a full MC simulation based on Geant4 [9,10] including decay-particle tracking, scintillation photon processes, and finite PMT timing resolution. This MC simulation reproduces the observed vertex distance

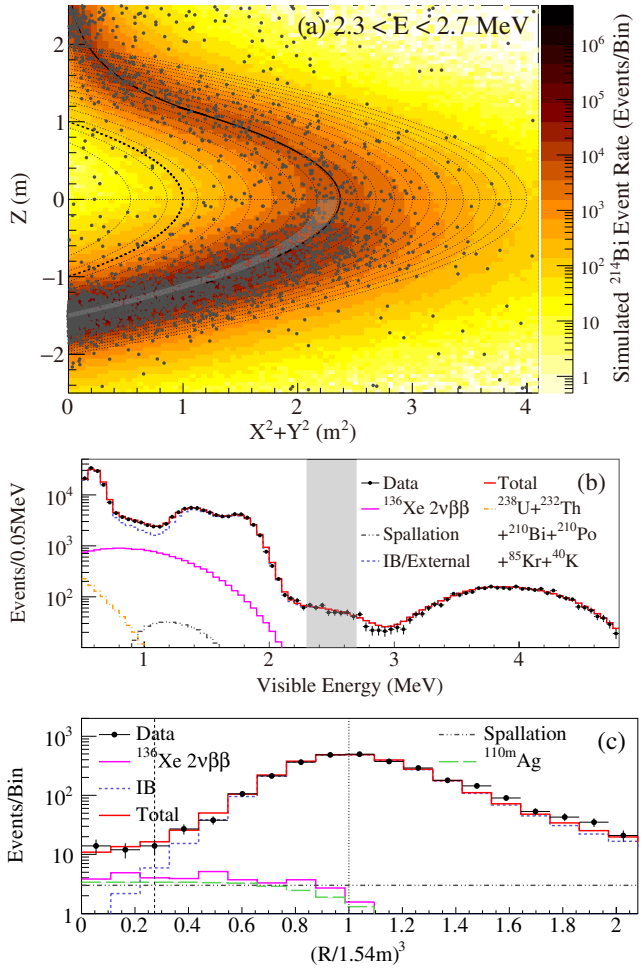

FIG. 1. (a) Vertex distribution of candidate events (black points) and reproduced ^{214}Bi background events in a Monte Carlo (MC) simulation (color histogram) for $2.3 < E < 2.7$ MeV (the $0\nu\beta\beta$ window). The normalization of the MC event histogram is arbitrary. The solid and thick dashed lines indicate the shape of the IB and the 1-m-radius spherical volume, respectively. The thin dashed lines illustrate the shape of the equal-volume spherical half shells that compose the 2-m-radius spherical fiducial volume for the $0\nu\beta\beta$ analysis. (b) An example of the energy spectrum in a volume bin with high ^{214}Bi background events around the lower part of the IB film [shaded region in (a) at $1.47 < R < 1.53$ m, $z < 0$]. (c) R^3 vertex distribution of candidate events in the $0\nu\beta\beta$ window. The curves show the best-fit background model components.

between ^{214}Bi and ^{214}Po sequential decay events from the initial ^{222}Rn contamination within the Xe-LS.

An enlarged 3.5-m-radius spherical volume was used to study a high statistics sample of muon spallation products and better constrain their background contributions. This included a region outside the IB. We assess a 22% systematic uncertainty on the calculated spallation yields in the Xe-LS, taking account of the observed $(20 \pm 2)\%$ increase in the spallation-neutron flux in the Xe-LS relative to the outer LS. In the $0\nu\beta\beta$ window, events from ^{10}C decays (β^+, $\tau = 27.8$ s, $Q = 3.65$ MeV) dominate the contribution from muon spallation. A triple-coincidence tag of a muon, a neutron identified by neutron-capture γ rays, and the ^{10}C decay [11], reduces the ^{10}C background with an efficiency of $(64 \pm 4)\%$. Post-muon spallation-neutron events are recorded by newly introduced dead-time free electronics. We apply spherical volume cuts ($\Delta R < 1.6$ m) around the reconstructed neutron vertices for 180 s after the preceding muon. We estimate that the remaining ^{10}C background after cuts is $(1.01 \pm 0.26) \times 10^{-2}$ (ton day)$^{-1}$, where ton is a unit of Xe-LS mass. Other shorter-lived products, e.g., ^{6}He and ^{12}B, are also reduced by the triple-coincidence tag and have a minor contribution to the background. The dead time introduced by all the spallation cuts is 7%. In the Xe-LS, long-lived ^{137}Xe (β^-, $\tau = 5.5$ min, $Q = 4.17$ MeV) is a background source produced by neutron capture on ^{136}Xe. Based on the spallation-neutron rate and the ^{136}Xe capture cross section [12], the production yield of ^{137}Xe is estimated to be $(3.9 \pm 2.0) \times 10^{-3}$ (ton day)$^{-1}$, which is consistent with the simulation study in FLUKA [13,14].

We perform the $0\nu\beta\beta$ decay analysis using a 2-m-radius fiducial volume (FV) as described above to utilize the deployed ^{136}Xe mass. However, the sensitivity is dominated by the innermost 1-m-radius spherical volume due to the background from the IB. The region outside this radius serves to strongly constrain the tails of the IB background extending into the innermost region. Further, anticipating the decay of the ^{110m}Ag background identified in phase I, we divide the phase-II data set into two equal time periods (period 1 and period 2), each roughly equal to one average lifetime of the ^{110m}Ag decay rate. Table I lists the number of observed events, and the estimated and best-fit background contributions in the $0\nu\beta\beta$ window within a 1-m-radius spherical volume for each of the two time periods. The fit is described in detail below. We find a precipitous decrease in the event rate in the $0\nu\beta\beta$ window in period 2. The period-2 background components are well constrained near the values listed in Table I with the exception of ^{110m}Ag. The hypothesis of standard radioactive decay of the $0\nu\beta\beta$ window background with the decay rate of ^{110m}Ag is disfavored relative to the hypothesis of a faster reduction at 96% C.L. The origin of this apparent reduction of ^{110m}Ag is unknown, but we speculate that much of it settled to the bottom of the IB where only a small fraction of ^{110m}Ag decays is reconstructed in the inner Xe-LS volume. In order to allow the $0\nu\beta\beta$ window background the greatest freedom in the fit, the $0\nu\beta\beta$ decay analyses are performed independently for period 1 and period 2.

The $2\nu\beta\beta$ decay rate can, in principle, be estimated from the same analysis used to derive the $0\nu\beta\beta$ decay limits, but the region outside of 1-m radius contributes negligibly to the $2\nu\beta\beta$ decay rate estimate and is dominated by systematic uncertainty arising from the IB background. To obtain a

TABLE I. Summary of the number of observed events, and the estimated and best-fit background contributions in the energy region $2.3 < E < 2.7$ MeV ($0\nu\beta\beta$ window) within the 1-m-radius spherical volume for each of the two time periods.

	Period-1 (270.7 days)		Period-2 (263.8 days)	
Observed events	22		11	
Background	Estimated	Best-fit	Estimated	Best-fit
^{136}Xe $2\nu\beta\beta$	...	5.48	...	5.29
Residual radioactivity in Xe-LS				
^{214}Bi (^{238}U series)	0.23 ± 0.04	0.25	0.028 ± 0.005	0.03
^{208}Tl (^{232}Th series)	...	0.001	...	0.001
^{110m}Ag	...	8.5	...	0.0
External (Radioactivity in IB)				
^{214}Bi (^{238}U series)	...	2.56	...	2.45
^{208}Tl (^{232}Th series)	...	0.02	...	0.03
^{110m}Ag	...	0.003	...	0.002
Spallation products				
^{10}C	2.7 ± 0.7	3.3	2.6 ± 0.7	2.8
^{6}He	0.07 ± 0.18	0.08	0.07 ± 0.18	0.08
^{12}B	0.15 ± 0.04	0.16	0.14 ± 0.04	0.15
^{137}Xe	0.5 ± 0.2	0.5	0.5 ± 0.2	0.4

$2\nu\beta\beta$ decay rate free of such systematic uncertainty, we perform a separate estimate using a likelihood fit to the binned energy spectrum of the selected candidates between 0.5 and 4.8 MeV, limited to a volume within the 1-m-radius spherical fiducial volume ($FV_{2\nu}$). The corresponding fiducial exposure of ^{136}Xe is 126 kg yr. The contributions from major backgrounds in the Xe-LS, such as ^{85}Kr, ^{40}K, ^{210}Bi, and the ^{228}Th-^{208}Pb subchain of the ^{232}Th series are free parameters and are left unconstrained in the spectral fit. We confirmed that the ^{134}Cs contribution in the Xe-LS is negligible from a fit. The contributions from the ^{222}Rn-^{210}Pb subchain of the ^{238}U series, muon spallation products, and detector energy response model parameters are allowed to vary but are constrained by their independent estimations. The $2\nu\beta\beta$ decay rates for period 1 and period 2 are $100.1^{+1.1}_{-1.8}\,(\text{ton day})^{-1}$ and $100.1^{+1.0}_{-0.9}\,(\text{ton day})^{-1}$, respectively, and are in agreement within the statistical uncertainties. The resolution tail in $2\nu\beta\beta$ decays is an important background in the $0\nu\beta\beta$ analysis. Such tail events are reproduced in ^{214}Bi decays with high-Rn data assuming the Gaussian resolution, indicating that a contribution from energy reconstruction failures is negligible.

We assess the systematic uncertainty of the $FV_{2\nu}$ cut based on the study of uniformly distributed ^{214}Bi events from initial ^{222}Rn contamination throughout the Xe-LS. We obtain a 3.0% systematic error on $FV_{2\nu}$, consistent with the 1.0 cm radial vertex bias in the source calibration data. Other sources of systematic uncertainty, such as xenon mass (0.8%), detector energy scale (0.3%) and efficiency (0.2%), and ^{136}Xe enrichment (0.09%), only have a small contribution; the overall uncertainty is 3.1%. The measured $2\nu\beta\beta$ decay half-life of ^{136}Xe is $T^{2\nu}_{1/2} = 2.21 \pm 0.02(\text{stat}) \pm 0.07(\text{syst}) \times 10^{21}$ yr. This result is consistent with our previous result based on phase-I data, $T^{2\nu}_{1/2} = 2.30 \pm 0.02(\text{stat}) \pm 0.12(\text{syst}) \times 10^{21}$ yr [15], and with the result obtained by EXO-200, $T^{2\nu}_{1/2} = 2.165 \pm 0.016(\text{stat}) \pm 0.059(\text{syst}) \times 10^{21}$ yr [16].

For the $0\nu\beta\beta$ analysis, using the larger 2-m-radius FV, the dominant ^{214}Bi background on the IB is radially attenuated but larger in the lower hemisphere. So we divide the FV into 20 equal-volume bins for each of the upper and lower hemispheres [see Fig. 1(a)]. We perform a simultaneous fit to the energy spectra for all volume bins. The z dependence of ^{214}Bi on the IB film is extracted from a fixed energy window dominated by these events. The ^{214}Bi background contribution is then broken into two independent distributions in the upper and lower hemispheres whose normalizations are floated as free parameters. The fit reproduces the energy spectra for each volume bin; Fig. 1(b) shows an example of the energy spectrum in a volume bin with high ^{214}Bi background events around the IB film. The radial dependences of candidate events and best-fit background contributions in the $0\nu\beta\beta$ window are illustrated in Fig. 1(c). The possible background contributions from ^{110m}Ag are free parameters in the fit. We consider three independent components: ^{110m}Ag uniformly dispersed in the Xe-LS volume, and on the surfaces of each the lower and upper IB films. We also examined nonuniform ^{110m}Ag sources, with different assumed radial dependences, in the Xe-LS but determined that this has little impact on the $0\nu\beta\beta$ limit.

As described above, the fits are performed independently for period 1 and period 2 in the region $0.8 < E < 4.8$ MeV. We found no event excess over the background expectation for both data sets. The 90% C.L. upper limits on the ^{136}Xe $0\nu\beta\beta$ decay rate are $< 5.5\,(\text{kton day})^{-1}$ and $< 3.4\,(\text{kton day})^{-1}$ for period 1 and period 2, respectively.

To demonstrate the low background levels achieved in the $0\nu\beta\beta$ region, Fig. 2 shows the energy spectra within a 1-m radius, together with the best-fit background composition and the 90% C.L. upper limit for $0\nu\beta\beta$ decays. Combining the results, we obtain a 90% C.L. upper limit of $< 2.4\,(\text{kton day})^{-1}$, or $T^{0\nu}_{1/2} > 9.2 \times 10^{25}$ yr (90% C.L.). We find that a fit including potential backgrounds from ^{88}Y, ^{208}Bi, and ^{60}Co [3] does not change the obtained limit. A MC of an ensemble of experiments assuming the best-fit background spectrum without a $0\nu\beta\beta$ signal indicates a sensitivity of 5.6×10^{25} yr, and the probability of obtaining a limit stronger than the presented result is 12%. For comparison, the sensitivity of an analysis in which the ^{110m}Ag background rates in period 1 and period 2 are constrained to the ^{110m}Ag half-life is 4.5×10^{25} yr.

Combining the phase-I and phase-II results, we obtain $T^{0\nu}_{1/2} > 1.07 \times 10^{26}$ yr (90% C.L.). This corresponds to an almost sixfold improvement over the previous KamLAND-Zen limit using only the phase-I data, owing to a significant reduction of the ^{110m}Ag contaminant and the increase in the exposure of ^{136}Xe.

From the limit on the ^{136}Xe $0\nu\beta\beta$ decay half-life, we obtain a 90% C.L. upper limit of $\langle m_{\beta\beta}\rangle < (61 - 165)$ meV using an improved phase space factor calculation [17,18] and commonly used NME calculations [19–25] assuming the axial coupling constant $g_A \simeq 1.27$. Figure 3 illustrates the allowed range of $\langle m_{\beta\beta}\rangle$ as a function of the lightest neutrino mass m_{lightest} under the assumption that the decay mechanism is dominated by exchange of a pure-Majorana Standard Model neutrino. The shaded regions include the uncertainties in U_{ei} and the neutrino mass splitting, for each hierarchy. Also drawn are the experimental limits from the $0\nu\beta\beta$ decay searches for each nucleus [2,26–28]. The upper limit on $< m_{\beta\beta} >$ from KamLAND-Zen is the most stringent, and it also provides the strongest constraint on m_{lightest} considering extreme cases of the combination of CP phases and the uncertainties from neutrino oscillation parameters [29,30]. We obtain a 90% C.L. upper limit of $m_{\text{lightest}} < (180\text{–}480)$ meV.

In conclusion, we have demonstrated effective background reduction in the Xe-loaded liquid scintillator by purification, and enhanced the $0\nu\beta\beta$ decay search sensitivity in KamLAND-Zen. Our search constrains the mass

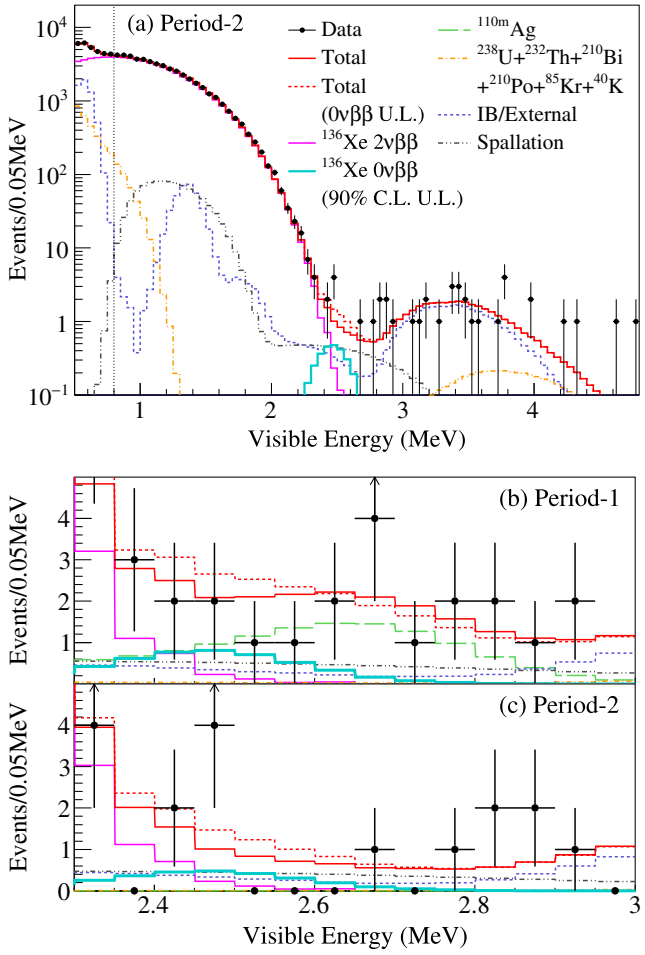

FIG. 2. (a) Energy spectrum of selected $\beta\beta$ candidates within a 1-m-radius spherical volume in period 2 drawn together with best-fit backgrounds, the $2\nu\beta\beta$ decay spectrum, and the 90% C.L. upper limit for $0\nu\beta\beta$ decay. [(b) and (c)] Close-up energy spectra for $2.3 < E < 3.0$ MeV in period 1 and period 2, respectively.

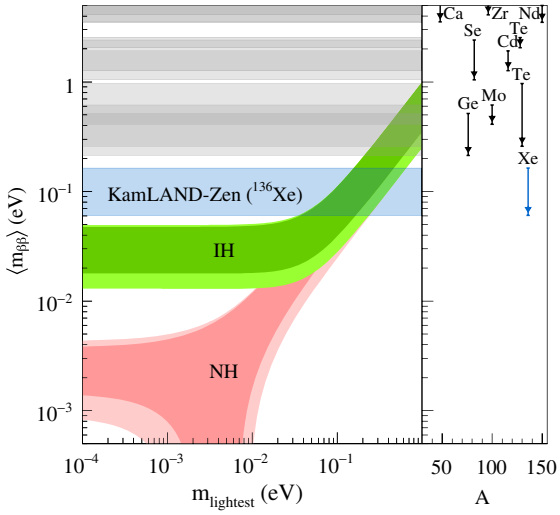

FIG. 3. Effective Majorana neutrino mass $\langle m_{\beta\beta}\rangle$ as a function of the lightest neutrino mass m_{lightest}. The dark shaded regions are the predictions based on best-fit values of neutrino oscillation parameters for the normal hierarchy (NH) and the inverted hierarchy (IH), and the light shaded regions indicate the 3σ ranges calculated from the oscillation parameter uncertainties [29,30]. The horizontal bands indicate 90% C.L. upper limits on $\langle m_{\beta\beta}\rangle$ with ^{136}Xe from KamLAND-Zen (this work), and with other nuclei from Refs. [2,26–28], considering an improved phase space factor calculation [17,18] and commonly used NME calculations [19–25]. The side panel shows the corresponding limits for each nucleus as a function of the mass number.

scale to lie below ~100 meV, and the most advantageous nuclear matrix element calculations indicate an effective Majorana neutrino mass limit near the bottom of the quasidegenerate neutrino mass region. The current KamLAND-Zen search is limited by backgrounds from ^{214}Bi, ^{110m}Ag, and muon spallation, and partially by the tail of $2\nu\beta\beta$ decays. In order to improve the search sensitivity, we plan to upgrade the KamLAND-Zen experiment with a larger Xe-LS volume loaded with 800 kg of enriched Xe, corresponding to a twofold increase in ^{136}Xe, contained in a larger balloon with lower radioactive background contaminants. If further radioactive background reduction is achieved, the background will be dominated by muon spallation, which can be further reduced by optimization of the spallation cut criteria. Such an improved search will allow $\langle m_{\beta\beta}\rangle$ to be probed below 50 meV, starting to constrain the inverted mass hierarchy region under the assumption that neutrinos are Majorana particles. The sensitivity of the experiment can be pushed further by improving the energy resolution to minimize the leakage of the $2\nu\beta\beta$ tail into the $0\nu\beta\beta$ analysis window. Such improvement is the target of a future detector upgrade.

The authors wish to acknowledge Professor A. Piepke for providing radioactive sources for KamLAND. The KamLAND-Zen experiment is supported by JSPS KAKENHI Grants No. 21000001 and No. 26104002; the World Premier International Research Center Initiative (WPI Initiative), MEXT, Japan; Stichting FOM in the Netherlands; and under the U.S. Department of Energy (DOE) Contract No. DE-AC02-05CH11231, as well as other DOE and NSF grants to individual institutions. The Kamioka Mining and Smelting Company has provided service for activities in the mine. We acknowledge the support of NII for SINET4.

[1] S. Dell'Oro, S. Marcocci, M. Viel, and F. Vissani, Adv. High Energy Phys. **2016**, 2162659 (2016).
[2] M. Agostini *et al.* (GERDA Collaboration), Phys. Rev. Lett. **111**, 122503 (2013).
[3] A. Gando *et al.* (KamLAND-Zen Collaboration), Phys. Rev. Lett. **110**, 062502 (2013).
[4] J. Albert *et al.* (EXO Collaboration), Nature (London) **510**, 229 (2014).
[5] A. Gando *et al.* (KamLAND Collaboration), Phys. Rev. C **92**, 055808 (2015).
[6] A. Gando *et al.* (KamLAND Collaboration), Phys. Rev. D **88**, 033001 (2013).
[7] S. Abe *et al.* (KamLAND Collaboration), Phys. Rev. C **84**, 035804 (2011).
[8] A. Gando *et al.* (KamLAND-Zen Collaboration), Phys. Rev. C **85**, 045504 (2012).
[9] S. Agostinelli *et al.*, Nucl. Instrum. Methods Phys. Res., Sect. A **506**, 250 (2003).
[10] J. Allison *et al.*, IEEE Trans. Nucl. Sci. **53**, 270 (2006).
[11] S. Abe *et al.* (KamLAND Collaboration), Phys. Rev. C **81**, 025807 (2010).
[12] J. B. Albert *et al.*, arXiv:1605.05794v1.
[13] G. Battistoni, F. Cerutti, A. Fassò, A. Ferrari, S. Muraro, J. Ranft, S. Roesler, and P. R. Sala, AIP Conf. Proc. **896**, 31 (2007).
[14] A. Ferrari, P. R. Sala, A. Fassó, and J. Ranft, *FLUKA: A Multiparticle Transport Code* (CERN, Geneva, 2005).
[15] A. Gando *et al.* (KamLAND-Zen Collaboration), Phys. Rev. C **86**, 021601 (2012).
[16] J. B. Albert *et al.* (EXO Collaboration), Phys. Rev. C **89**, 015502 (2014).
[17] J. Kotila and F. Iachello, Phys. Rev. C **85**, 034316 (2012).
[18] S. Stoica and M. Mirea, Phys. Rev. C **88**, 037303 (2013); updated in arXiv:1411.5506v3.
[19] T. R. Rodríguez and G. Martínez-Pinedo, Phys. Rev. Lett. **105**, 252503 (2010).
[20] J. Menéndez, A. Poves, E. Caurier, and F. Nowacki, Nucl. Phys. **A818**, 139 (2009).
[21] J. Barea, J. Kotila, and F. Iachello, Phys. Rev. C **91**, 034304 (2015).
[22] J. Hyvärinen and J. Suhonen, Phys. Rev. C **91**, 024613 (2015).
[23] A. Meroni, S. T. Petcov, and F. Šimkovic, J. High Energy Phys. 02 (2013) 025.
[24] F. Šimkovic, V. Rodin, A. Faessler, and P. Vogel, Phys. Rev. C **87**, 045501 (2013).
[25] M. T. Mustonen and J. Engel, Phys. Rev. C **87**, 064302 (2013).
[26] K. Alfonso *et al.* (CUORE Collaboration), Phys. Rev. Lett. **115**, 102502 (2015).
[27] R. Arnold *et al.* (NEMO-3 Collaboration), Phys. Rev. D **92**, 072011 (2015).
[28] A. S. Barabash, Phys. At. Nucl. **74**, 603 (2011).
[29] S. Dell'Oro, S. Marcocci, and F. Vissani, Phys. Rev. D **90**, 033005 (2014).
[30] F. Capozzi, G. L. Fogli, E. Lisi, A. Marrone, D. Montanino, and A. Palazzo, Phys. Rev. D **89**, 093018 (2014).